coatings

MDPI

Article

Mechanical Performance and Strengthening Mechanism of Polymer Concretes Reinforced with Carbon Nanofiber and Epoxy Resin

Zhenfang Li, Aizhu Liu, Dong Gao, Chuanji Wu, Xin Liu and Haoran Zhai *

Shandong High-Speed Urban and Rural Development Group Co., Ltd., Jinan 250013, China; cxfzlizhenfang@126.com (Z.L.); cxfzazliu@163.com (A.L.); cxfzdgao@163.com (D.G.); cxfzcjwu@163.com (C.W.); cxfzxliu@163.com (X.L.)
* Correspondence: cxfzzhaihaoran@163.com

Abstract: To address the issues of the brittleness, low tensile strength, insufficient bond strength, and reduced service life associated with ordinary cement concrete being used as a repair material, a water-based epoxy (WBE) and carbon-nanofiber-reinforced concrete composite repair material was designed, and the mechanical properties, bonding performance, and durability of the concrete modified using WBE and carbon fiber under various WBE contents were investigated and evaluated. In this paper, a self-emulsifying water-based epoxy curing agent with reactive, rigid, flexible, and water-soluble chains was obtained via chemical grafting, involving the incorporation of polyethylene glycol chain segments into epoxy resin molecules. The results demonstrated that a WBE has a contributing effect on improving the weak interfacial bond between the carbon fiber and concrete; moreover, the composite admixture of carbon fiber and WBE improves the mechanical properties and durability of concrete, in which the composite admixture of 1% carbon fiber and 10% WBE has the best performance. The flexural strength and chlorine ion permeability resistance of concrete were slightly reduced after more than 10% admixture, but bond strength, tensile strength, compressive strength, dry shrinkage resistance, and frost resistance were promoted. The addition of WBE significantly retards the cement hydration process while greatly improving the compactness and impermeability of the concrete. Furthermore, the combined effects of WBE and carbon fiber effectively prevented the generation and expansion of cracks. The interaction mechanism and microstructure evolution between the WBE, carbon fiber, and cement hydration were described by clarifying the mineral composition, organic–inorganic interactions, the evolution of the hydration products, and composite morphology at different scales. Carbon fiber and WBE exhibited synergistic effects on the tensile strength, ductility, and crack resistance of concrete. In the formed three-dimensional network structural system of concrete, the WBE formed an organic coating layer on the fiber surface and provided fiber protection as well as interfacial bonding reinforcement for the embedded cement particles.

Keywords: concrete; water-based epoxy; carbon nanofiber; mechanical properties; durability

1. Introduction

As a cement-based material, concrete plays an important role in construction and building maintenance. Because of the main performance disadvantages of concrete, such as poor toughness, insufficient crack resistance, and low-durability performance, it limits its wide utilization in engineering fields. Especially, in some cold areas, the probability of frost damage to concrete is greater. The stress damage caused by the freeze–thaw cycle within the concrete matrix results in a noteworthy strength reduction, thus affecting the service life of concrete. However, due to the prolonged service stage and variable environmental factors, concrete structures are susceptible to damage due to spalling and cracking, surface peeling, and even fatigue collapse [1,2], leading to the aggravation of corrosion. Every year, direct economic losses are up to 300 billion because of concrete deterioration, posing

a threat to national safety production. Damage to concrete structures typically occurs in areas of stress concentration (e.g., steps, joints, edges) and cyclic deformation zones (e.g., corrosive environments, freeze–thaw pavements, piers, and bridges). In response to increasingly demanding requirements, concrete requires continuous advancement to ensure the safety and reliability of its associated structures.

The introduction of polymeric materials such as liquid resins, dispersed polymer powders, latexes, waterborne polymers, etc. into concrete has now been a widespread concern in the field of civil engineering [3,4]. It has been found that the incorporation of these polymers improves the bond strength, mechanical strength, impermeability, chemical resistance, and durability of the cementitious composites [5]. Studies have revealed that the physical filling effect of polymers on the porosity of cementitious composites is the primary modification mechanism of polymer-modified concrete. The addition of polymers not only fills the holes in the concrete and reduces its porosity, but it also improves the tensile strength and prevents the expansion of microcracks. In addition, the appropriate amount of incorporation to form dispersed polymers could form a film wrapping around the cement hydrate and aggregate to produce an interpenetrating network structure. This three-dimensional polymer film plays an important role in bridging concrete microcracks and improving concrete toughness.

In recent decades, a growing development in the concrete repair industry has been to generate various repair systems, including cement repair systems [6,7], polymer repair systems [8,9], cement–polymer composite repair systems [10,11], steel plate bonding repair systems [12], and fiber-reinforced repair systems [13]. Among these, epoxy concrete has gained widespread popularity due to its superior mechanical properties, chemical stability, construction operability, and higher bond strength, as compared to other repair systems [14,15]. However, a solvent-based epoxy resin is commonly employed as polymer in epoxy concrete. As an oil-soluble polymer, it is inherently insoluble with the water-soluble system of cement concrete. Consequently, there are several issues associated with the poor synergy between epoxy polymerization and cement hydration, such as oil–water separation, leading to the severe delamination and instability of the network interpenetration structure. Additionally, a large number of free organic solvents hinder cement hydration, further complicating the formation compound between solvent-based epoxy resin and cement concrete. Despite the advantages of its prominent mechanical properties, high adhesive strength, and fast curing, the inherent disadvantages of solvent-based epoxy resin, such as susceptible aging, a short application period, high cost, and toxicity, limits its broad application prospects in large-scale repair operations. Especially for large-volume mixing, solvent-based epoxy resin has the characteristics of high viscosity and poor compatibility in low-temperature environments. Meanwhile, in high-temperature environments, it is prone to burst aggregation, agglomeration, rapid condensation, and difficulty in controlling its work performance and construction quality [16]. Therefore, the practical application of solvent-based epoxy resin in large-scale repair operations is severely limited.

Water-based epoxy resin is a novel type of epoxy resin system that utilizes water as the dispersed phase, instead of organic solvents. The resin system has several dominant properties, such as mutual solubility with water in any proportion, excellent flexibility, low toxicity, an extended application period, and room-temperature curing. Additionally, water-based epoxy exhibits exceptional adhesion on wet surfaces, and the drying treatment for old concrete bonding surfaces is unnecessary [17,18]. However, water-based resins have the disadvantage of the high latent heat deriving from evaporation, which promotes the molecular polymerization of a cross-linking curing reaction with an inefficient reaction rate. Furthermore, water-soluble functional groups like sodium sulfonic acid, sodium sulfate, sodium carboxylate, and amine groups are introduced into the main chain of water-based epoxy resin molecules not involved in polymerization, resulting in the film formation rate, mechanical properties, and aging resistance decreasing as well. Therefore, epoxy resin polymerization with cement hydration in a water-based epoxy–concrete composite repair system is incorporated. This composite repair system leverages the respective advantages

of water-based epoxy and concrete, while compensating for their shortcomings as well. During the reaction process, cement hydration consumes water and accordingly reduces the latent heat of evaporation, further promoting the cross-linking and curing of epoxy resin. Thus, the compressive strength, elastic modulus, and aging resistance of the resin is notably improved, and the drawbacks of water-based epoxy are effectively compensated for as well. After film formation, a polymer network interpenetrating structure matrix stemming from the water-based epoxy is fabricated, which fills the defects and pores in the concrete as a continuous phase and enhances the bond strength, tensile strength, ductility, and durability of the concrete [19,20].

In this paper, the grafting of polyethylene glycol-2000 (PEG-2000) into the chain segments of epoxy resin polymer (EP) was investigated, resulting in the introduction of hydrophilic polyoxyethylene chain segments into the molecular chains of EP, thereby obtaining a nonionic self-emulsifying waterborne epoxy resin (WBE). The incorporation of WBE, carbon fiber, a curing agent, and aggregate was adjusted to obtain WBE-modified concrete materials using different polymer admixtures. The mechanical pattern and durability of the resulting WBE–concrete composite repair materials were systematically studied, specifically in terms of compressive strength, flexural strength, tensile strength, bond strength, penetration resistance, chloride salt resistance, freeze–thaw resistance, and shrinkage. The effects of the polymer admixture and fiber on the performance of the modified concrete were analyzed.

2. Materials and Methods

2.1. Raw Materials

The cement utilized in the study is P.O 42.5 ordinary silicate cement manufactured by Shanshui Group (Jinan, China). The fundamental characteristics of the cement are presented in Table 1 complying with ASTM C-150. The short-cut carbon fiber as the reinforcement in the concrete matrix was obtained from Toray Industries, Japan, and the primary performance indicators are presented in Table 2 and Figure 1. Additionally, the preferred high-efficiency water reducing agent utilized is the polycarboxylic acid type produced by construction material company Jiangsu Botte, which boasts a water reduction rate of 30%.

Table 1. Properties of ordinary portland cement.

Items	National Standard	Measured Results
Fineness ($m^2 \cdot kg^{-1}$)	300	360
Initial setting time (min)	≥ 45	235
Final setting time (min)	≤ 600	400
Soundness (boiling) (mm)	≤ 5	2.0
3 d flexural strength (MPa)	≥ 3.5	5.0
28 d flexural strength (MPa)	≥ 6.5	8.5
3 d compressive strength (MPa)	≥ 17.0	19.0
28 d compressive strength (MPa)	≥ 42.5	49.5

Table 2. Performance parameters of carbon fiber.

Filament Diameter (μm)	Tensile Strength (GPa)	Tensile Modulus (GPa)	Carbon Content (%)	Elongation (%)	Density (g·cm³)	Volume Resistivity
7–10	3.57	246	97	1.6	1.79	35

Figure 1. The photo and SEM image of carbon fiber. The photo (**a**) and SEM (**b**) image of carbon fiber.

The fabrication process of the aqueous epoxy resin involved several steps. Firstly, 100 g of epoxy resin and toluene diisocyanate in a 1:1 mass ratio were subjected to continuous stirring for 2 h at 80 °C under the protection of N_2 until complete reaction. Subsequently, 50 g of PEG-2000 was added dropwise to the above solution, and the reaction was carried out for 1 h. Finally, the reaction product was cooled to 50 °C, and deionized water was gradually added along with rapid stirring until the viscosity of the system stabilized. At this point, the WBE was obtained with a solid content of ≥50%. The viscosity of the final product was 2150 mPa·s at 25 °C, and its specific characteristic indexed are detailed in Table 3.

Table 3. Basic characteristic indexes of WBE.

Indexes	WBE
Density (g·cm^{-3})	1.25
Solid content (%)	58
Epoxy equivalent (g/eq)	215~248
Viscosity (mPa·s)	2150

2.2. Preparation of Polymer-Modified Concrete

(1)   Proportional design of polymer-modified concrete

Based on the literature, the polymer admixture content is a crucial factor influencing cement hydration. A higher proportion of polymer admixture to cement ratio significantly impedes the cement hydration process and leads to a prolonged setting time. Therefore, an optimal polymer/cement ratio was prominent for ensuring the desired performance of the polymer-modified concrete. In this study, different polymer admixtures (5%, 10%, 20%) were used to form experimental groups, while a control group with no admixture was also included. The water–cement ratio (W/C) was another essential factor impacting the concrete's strength and durability. A low W/C ratio affected the concrete workability, while a high ratio caused excessive shrinkage and significant water loss. According to the present research, the W/C ratio was fixed at 0.33 after multiple trials, which referred to the water content in the water-based epoxy and admixture mixing. The content of water-reducing agent and carbon fiber admixture was both 1.0 wt.%. The mixing proportions of the concrete constituents are presented in Table 4.

(2)   Fabrication of polymer-modified concrete

The WBE–concrete hybrid repair material comprised cement concrete and WBE components. Water solubility was achieved by grafting hydrophilic chain segments into the WBE. Due to the self-emulsifying nature of WBE, it conferred water solubility after mixing. The high solid content and viscosity of the WBE hindered complete integration with the cement concrete. As a consequence, it was imperative to uniformly blend and disperse the WBE adhesive with water to create a consistent dispersion.

Table 4. The mix ratio of WBE-modified concrete.

Sample	P/C (wt.%)	W/C	Cement (kg/m^3)	Sand (kg/m^3)	Stone (kg/m^3)	Water (kg/m^3)	Water Reducer (%)	WBE (kg/m^3)	Carbon Fiber (wt.%)
C	0		500			165		0	0
CF									1
W5C	5		515			170		25	0
W5CF		0.33		650	1400		1		1
W10C	10		530			175		53	0
W10CF									1
W20C	20		560			185		112	0
W20CF									1

Firstly, the cement, aggregate, and fiber were weighed and mixed for 1 min to form a homogeneous mixture. The total amount of water required was divided into two portions, with one portion mixed with reducing agent for mixing the concrete while the other was used for diluting the WBE. Next, the water-reducing agent mixture was gradually added for 3 min to produce the concrete mixture. Then, the WBE was weighed and stirred for 30 s to fabricate a white viscous emulsion. Subsequently, the remaining half of water was added and stirred for another minute to form a thin emulsion of WBE. Finally, the WBE emulsion was poured into the concrete mixture and mixed for 3 min to achieve a uniform WBE-modified concrete mixture.

Casting treatment: The obtained WBE-modified concrete composites were discharged and poured into molds with dimensions of 100 mm × 100 mm × 100 mm, Φ100 mm × 100 mm × 200 mm, 100 mm × 100 mm × 400 mm, and 100 mm × 100 mm × 515 mm and shrinkage molds, tensile dumbbell molds, impermeability molds, etc., and oscillation and smooth, laminate, and marked processing was conducted. After demolding, all specimens were placed in an environment with a relative humidity greater than 95% and a temperature of 20 ± 2 °C until the target age.

2.3. Characterization

The mechanical properties of the WBE-modified concrete were tested at a curing age of 28 days. The age of the samples for bond strength testing was more than 60 days. Shown in Figures 2 and 3 is a detailed demonstration of the construction process of the samples during the mixing, pouring, shaping, and testing.

Figure 2. Experimental instruments and samples: (**a**) Pressure testing machine, (**b**) concrete rapid freeze–thaw tester, (**c**) various specimens, (**d**) concrete mixer.
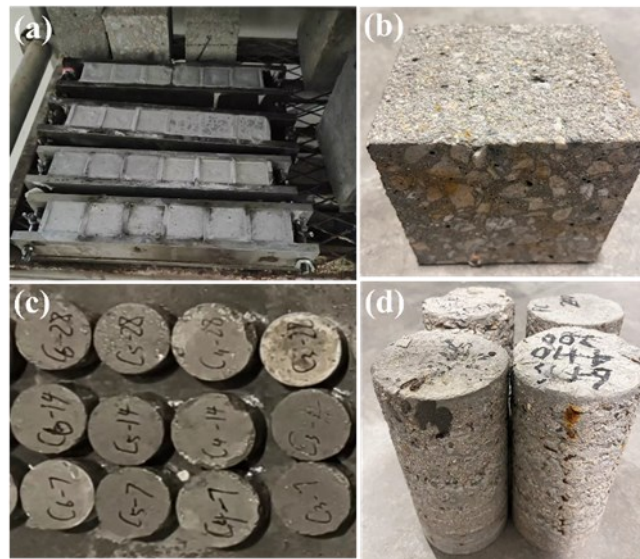
Figure 3. Various specimens for different measurements. (**a**) Bond strength test samples, (**b**) freeze-thaw samples, (**c**) chloride ion diffusion specimen, and (**d**) axial compressive strength test samples.

(1)   Compressive strength

Cylindrical specimens of Φ100 mm $\times$ 200 mm was used for concrete. The testing was displacement-controlled with a loading rate of 0.05 mm/min. There were 3 specimens evaluated in each group and averaged, and the results were accurate to 0.01 MPa. The strain gauges were examined to collect the strain values in the elastic deformation stage of the samples, and the displacement gauges were examined to collect the strain values in the yielding and breaking deformation stages of the samples. The stress–strain curve, modulus of elasticity, and Poisson's ratio of the concrete were calculated after the determination. The calculation method was as follows:

Modulus of elasticity: obtained from the ratio of 1/3 of the peak breaking stress (MPa) to the corresponding strain value and was accurate to 100 MPa; Poisson's ratio: taken from the ratio of the longitudinal strain to the transverse strain corresponding to the peak breaking stress.

(2)   Flexural strength

A four-point bending test was measured using a prismatic specimen with size of 100 mm $\times$ 100 mm $\times$ 400 mm. The testing method was in compliance with the standard GB-T 50081-2019, and controlled in displacement with a loading rate of 0.05 mm/min. There were 3 specimens conducted in each group and averaged with an accuracy of 0.01 MPa.

(3)   Tensile strength

The axial tensile strength of concrete was detected using a dumbbell-type tensile specimen with a loading rate of 0.05 mm/min. The test machine clamped a tensile screw, which was connected to a collet. The concrete specimen was clamped using the collet, which eventually produced tensile stress to destroy the specimen. The displacement sensor measured and output the axial tensile strain data with a measurement accuracy of 1×10^{-6}. The experiment results were valid if a crack broke through the middle of the specimen; otherwise, they were invalid.

(4)   Resistance to chloride ion permeability

The chloride ion permeability of the concrete was obtained using the electric flux method with a curing age of 28 days. The specimen size was 100 mm in diameter and 50 mm in height.

(5) Frost resistance

The frost resistance test method of concrete was conducted with the curing age of 28 days. The specimen size is 100 mm × 100 mm × 400 mm prismatic specimens. The freeze–thaw medium is tap water. The cycle period and number are 3.5 h and 300, respectively. The cycle temperature range is $-18 \pm 2 \,°C \sim 5 \pm 2 \,°C$. The mass loss and relative dynamic modulus were recorded every 25 cycles.

(6) Crystal structure and microscopic morphology analysis

The crystal structure characterization of WBE-modified concrete was performed using a D8 ADVANCE (Bruker, Mannheim, Germany) X-ray diffractometer. The samples detected were taken uniformly from the same batch and curing age, ground finely using an agate crucible, and sieved through 200 mesh. The microscopic morphology of the samples was acquired using a field emission scanning electron microscope (FE-SEM) GeminiSEM 500 (ZEISS, Oberkochen, Germany).

3. Results and Discussion

3.1. XRD Analyses of WBE-Modified Concrete

Figure 4 presents the X-ray diffraction (XRD) patterns of the concrete modified with WBE at different doses after a 28-day curing period. The results revealed that all materials exhibited diffraction peaks of calcium hydroxide (CH) at 18.2°, 34.1°, 47.3°, and 50.3°, tricalcium silicate (C_3S) at 29.2° and 32.1°, and dicalcium silicate (C_2S) at 27.9° [21]. No new diffraction peaks were detected in the WBE-modified concrete, indicating that the addition of epoxy resin did not generate new hydration products or affect the crystalline composition of the hydration products. Furthermore, the intensity of the C_3S and C_2S diffraction peaks decreased with an increasing WBE dosage, while the intensity of the CH diffraction peak raised. This suggested that the incorporation of WBE facilitated the hydration reaction, promoted the consumption of C_3S and C_2S derived from the cement raw materials, and accelerated the formation of CH and other hydration products. The combination of hydration products promoted a more adequate hydration reaction [22], thus in favor of an advancement of the mechanical performance of the concrete.
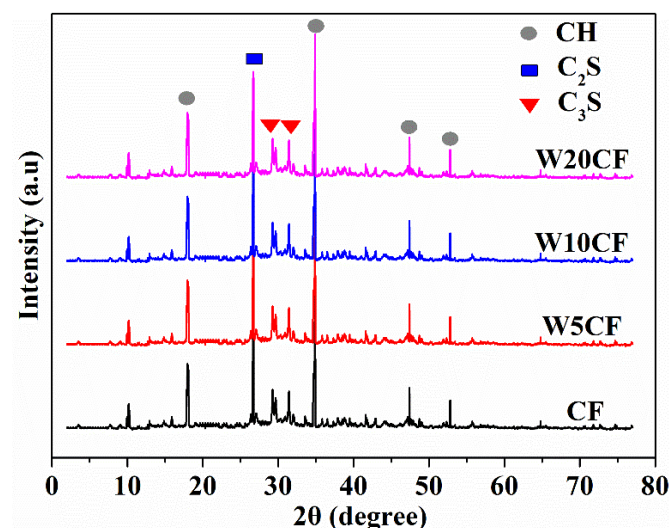

Figure 4. XRD patterns of various WBE-modified concrete types.

Figure 5 depicts the SEM micrographs of the WBE-modified concrete. In Figure 5a,b, in the absence of WBE, concrete exhibited a loose morphology, displaying discernible gaps and cracks. The presence of cement hydration products, namely calcium-silicate-hydrate (C-S-H), are visible in the pattern of rod-like and needle-like crystals (ettringite AFt phase). The abundant functional groups (hydroxyl, etc.) on the surface of the epoxy resin

provide sufficient points for crystal growth. The adsorbed Ca^{2+} lowered the concentration of Ca^{2+} in the solution and promoted the ionization process of the cement, resulting in the production of an excess of Ca^{2+} and OH^- in the solution. This effect promoted the formation of well-crystallized $Ca(OH)_2$ crystals, which are optimally oriented to grow along the crystal surface. The $Ca(OH)_2$ crystals are manifested in enlargement and thickening. The inadequate hydration of the cement led to insufficient pore filling via hydration products. Conversely, the images in Figure 5c–h show a highlighted increase in WBE doping, which significantly improved the structural denseness and reduced the number of cracks and pores. In Figure 5e, the concrete admixed with 10% epoxy resin (W10CF) exhibited the densest structure, the fewest cracks, a uniformly sized hydration product, and close packing of the hydration products around the aggregates. This could be attributed to the abundant functional groups on the chain segment of the WBE resin, which provided sufficient growth points for crystals. The hydration reaction was conducted more thoroughly and accelerated the production of calcium hydroxide. Similarly, a small number of crystal clusters of $CaCO_3$ can be observed in Figure 5f, mainly due to higher CO_2 concentrations or short-term carbonation. With further hydration of the cement, the polymer particles within the capillaries gradually agglomerated and flocculated together, forming a close layer on the surface of the cement gel [23,24]. In particular, the water between the polymer particles was absorbed to participate in the cement hydration, leading to the complete condensation and closure of the polymer particles on the mixture surface to form a continuous polymer reticular film. Figure 6 explains the chemical reaction between the polymer and cement hydration products, and the formation of a three-dimensional network structure. However, the SEM images in Figure 5g,h illustrated that when WBE doping up to 20% (W20CF), cracks were apparent, as was deterioration of the density. This could be attributed to the excessive epoxy resin encapsulation of aggregates hindering the hydration reaction. In Figure 5h, the polymer epoxy resin film presents network-like micelles, which are wrapped around each other after polymerization, with only a small amount of cement particles, hydration products, and carbon nanofibers embedded into them.
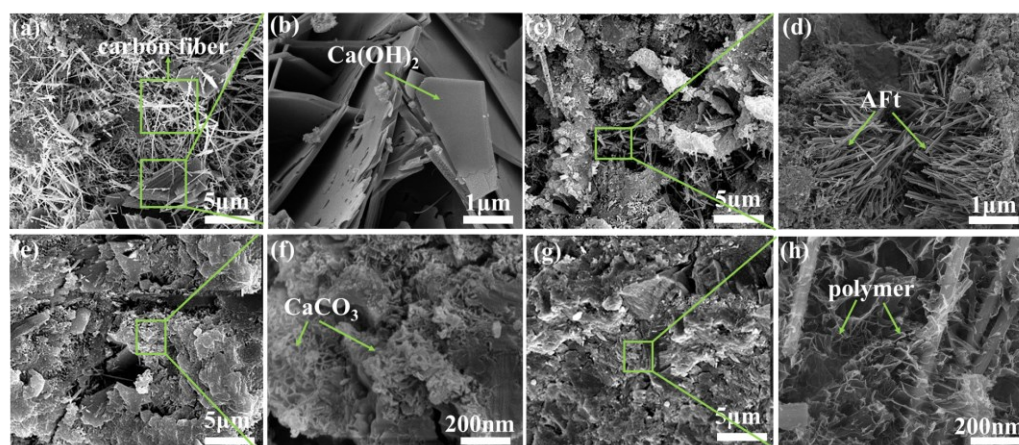

Figure 5. SEM images of WBE-modified concrete with varied WBE contents: (**a**,**b**) C, (**c**,**d**) W5CF, (**e**,**f**) W10CF, (**g**,**h**) W20CF.

3.2. Mechanical Properties Testing of Epoxy Resin Modified Concrete

Figure 7 displays the compressive strengths of WBE-modified concrete at curing ages of 3, 7, and 28 days. The compressive strengths exhibited a descending trend as the amount of WBE increased. This phenomenon can mainly be attributed to two major factors. Firstly, the strength of the epoxy resin WBE is considerably lower than that of the concrete matrix, which results in a longer curing reaction time. Consequently, the overall strength of concrete is reduced, and the polymer phase serves as a defect and stress concentration point during compression. Secondly, the air-entraining effect of the WBE on the concrete is strong. Thus, abundant air bubbles are generated during the mixing process, leading to

an increase in junction defects and the modified appearance of the structure in the loose phase after hardening. This structural change rendered it challenging for the concrete to withstand large loads. However, with the prolongation of the curing time, the epoxy resin was gradually cured along with the hydration of cement, and the compressive strength of the modified concrete was remarkably elevated. The difference in compressive strength between the modified concrete and blank concrete was progressively reduced [25].
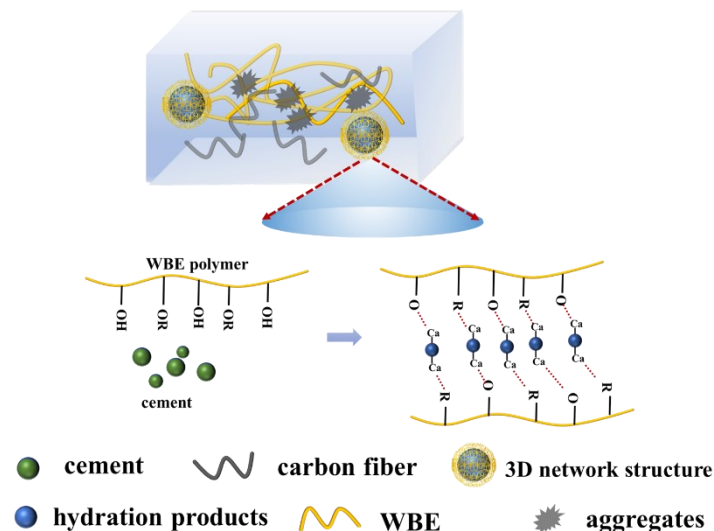
Figure 6. The chemical reaction of WBE with cement hydration products, and the formation of three-dimensional network structure.
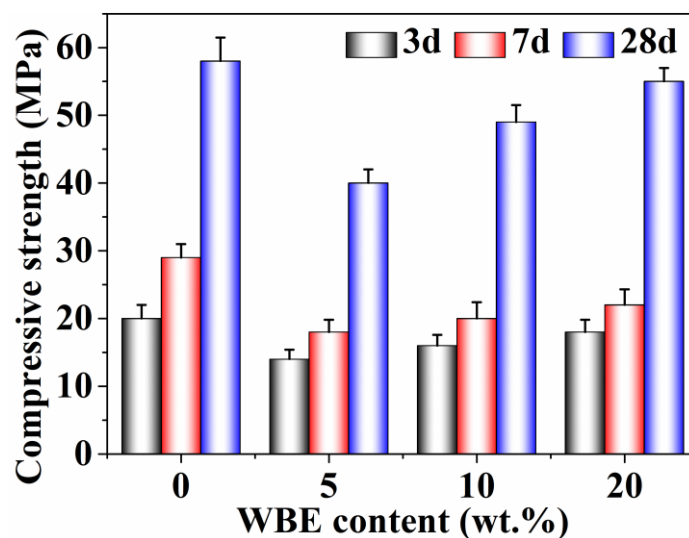

Figure 7. Compressive strength of WBE-modified concrete with various WBE contents.

Figure 8 presents the impact of different proportions of polymer WBE admixtures (0%, 5%, 10%, and 20%) and fiber fractions on the compressive strength of WBE-modified concrete. The stress–strain curves for each concrete specimen are depicted in Figure 8. The elastic modulus of the modified concrete gradually declined while the ductility and crack-arresting capacity were enhanced with the addition of WBE. Moreover, the compressive strength and elastic modulus of the modified concrete showed a downtrend with an increase in WBE. This behavior can primarily be attributed to the lower compressive strength and elastic modulus of WBE compared to the cement concrete matrix, leading to the greater susceptibility of WBE-modified concrete to deformation during compression. For concrete without WBE (Figure 8a), instability was more likely to occur in the yield-

ing stage, with cracks spreading rapidly through the matrix after reaching the ultimate compressive strength. Consequently, the force curve reduced rapidly, and the strength declined prominently to below 20%. However, the addition of the fiber does not effectively alleviate this phenomenon. In contrast, the decreasing section of the stress–strain curve was progressively smoothed coupled with the addition of WBE, and the toughening effect of the fiber components was more pronounced. These observations suggested that water-based epoxy (WBE) was a primary reason for the ductility enhancement of the concrete. Moreover, the crack resistance and toughening effect of the fiber component were more evident when it was used with WBE [26–28]. WBE improves the fiber dispersion and enhanced fiber pull-out effect via the encapsulating process. The cutting effect of the cement particles is alleviated as well.
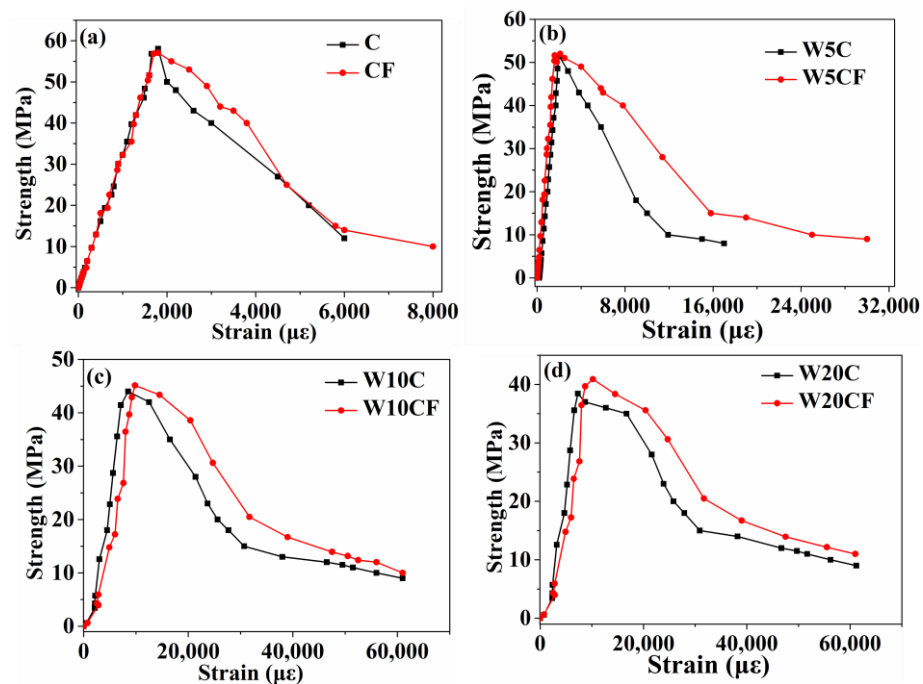

Figure 8. The 28-day compressive strength stress–strain curves of modified concrete with different WBE contents. (**a**) 0, (**b**) 5%, (**c**) 10%, (**d**) 20%.

Figure 9 illustrates the 28-day compressive Poisson's ratio curves of concrete specimens. The longitudinal and transverse strains of the specimens are shown on the horizontal and vertical coordinates, respectively. Each curve represents the upper and lower Poisson's limits of the measured concrete specimens. The solid green line indicates the fitted line of the elastic deformation process of the specimens, and its slope is calculated as Poisson's ratio. In Figure 9a, the transition of the compressive damage and matrix cracking of the unmodified plain concrete are staged, coupled with cracks occurring and expanding rapidly. With the addition of WBE, the deformation process of concrete was more stabilized (the upper and lower limits were closer) and the transition from the elastic phase to the yield phase was smoother (the curve deformation was smaller). This revealed that the crack extension was accompanied by a crack-blocking effect, which delayed the occurrence and further extension of cracks. Meanwhile, the high ductility and strong strain of the fiber reduced the occurrence of sudden collapse and loading force loss for the concrete matrix in the process of compressive deterioration. Overall, the WBE and carbon fiber provided improved confinement of the concrete matrix, and effective crack control [29].
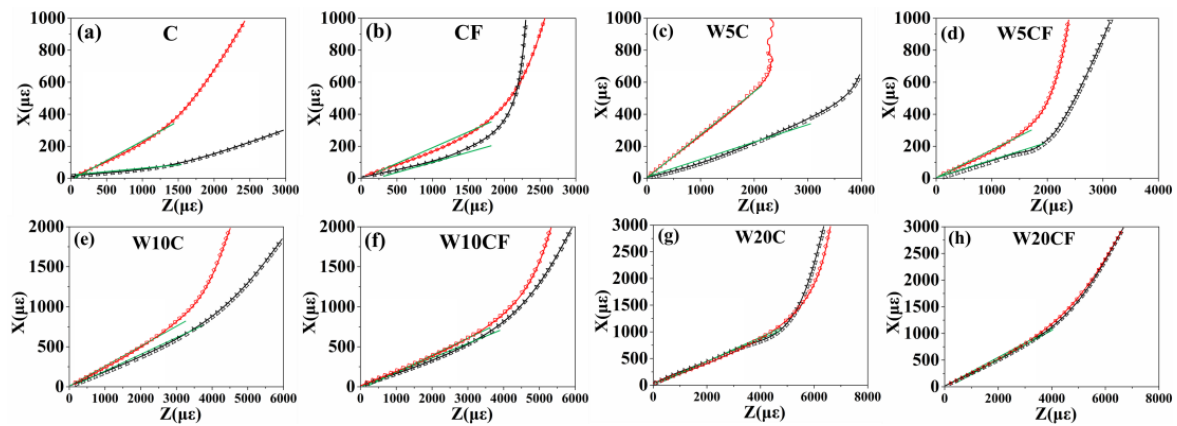
Figure 9. The 28-day compressive Poisson's ratio curves of modified concrete with various WBE contents. (**a**,**b**) 0, (**c**,**d**) 5% (**e**,**f**) 10%, (**g**,**h**) 20%.

Figure 10 presents the pertinent mechanical parameters derived from the compressive properties of concrete. The compressive strength and elastic modulus of the WBE-modified concrete exhibited a declining pattern. Conversely, Poisson's ratio demonstrated a rising trend, whereby the fiber component displayed no noteworthy influence on Poisson's ratio. Concerning the elastic modulus, fiber displayed a propensity to enhance the elastic modulus of conventional concrete, while an adverse effect was observed for WBE-modified concrete [30].
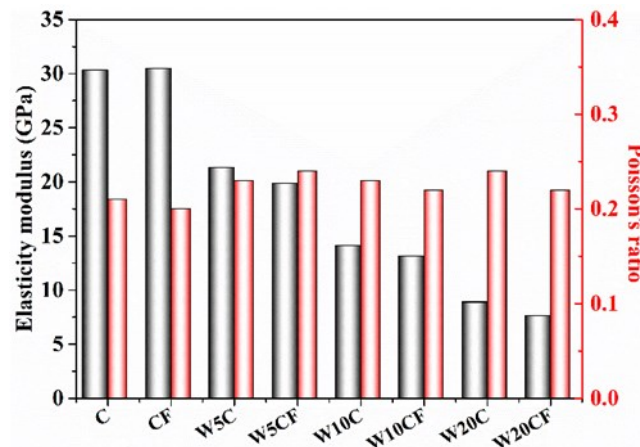

Figure 10. Poisson's ratio and elasticity modulus of WBE-modified concrete.

Figure 11 depicts the flexural strength of WBE-modified concrete with curing times of 3, 7, and 28 days. As illustrated in Figure 8, the flexural strengths of concrete with 0%, 5%, 10%, and 20% (mass fraction) WBE after 28 days were 7.5 MPa, 6.1 MPa, 8.1 MPa, and 7.2 MPa, respectively. The flexural strength of concrete exhibited an upward and then downward trend with an increasing amount of WBE. The maximum flexural strength was observed at 10% WBE. The observed enhancement can be attributed to the presence of abundant hydroxyl and oxy functional groups on the surface of the WBE, which exhibited excellent compatibility and contributed to the improvement of compressive and flexural strength of the concrete [31]. However, excessive WBE retarded the hydration reaction of the concrete by reducing the water content. In the meantime, a polymer film covering the surface of the aggregate and hydration products limits further hydration. Because the strength and elastic modulus of the polymerization film were relatively lower than that of the pure slurry, resulting in cracks or defects in the concrete matrix with exposure to stress, this ultimately negatively impacted its mechanical properties [32].
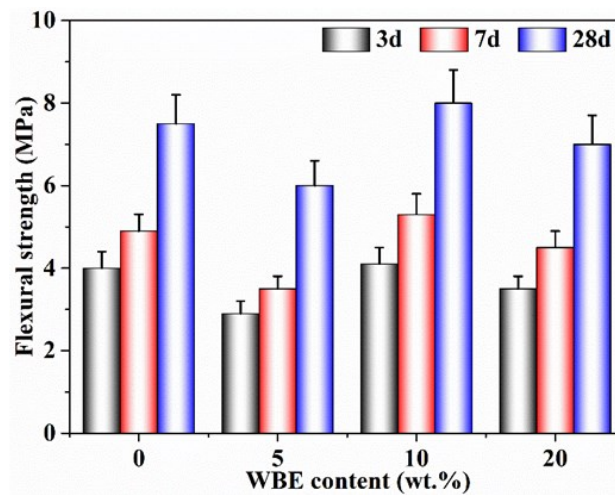
Figure 11. Flexural strength of WBE-modified concrete with various curing ages.

The flexural and crack resistance properties of the WBE-modified concrete could be evaluated by the ratio of the flexural to the compressive strength, where a higher ratio indicated greater flexibility and crack resistance. In Figure 12, the bending–compressive ratio of concrete declined with an extended curing age, which was the inevitable result of the cement gradually hardening into hard and brittle material during the curing process. However, the addition of a small amount of WBE could effectively enhance the anti-cracking performance of the concrete, leading to a higher bending–compressive ratio compared to the unmodified groups at all three ages studied. The highest ratio was observed in the 10% WBE dosing group with a curing age of 7 days, which was 65.62% higher than that of the unmodified group. This dramatic effect contributed to the WBE film serving as the primary modification structure, which bonded with the aggregate and hydration products, forming a more compact and flexible organic–inorganic composite mesh structure, in comparison with the single-hydration-product cohesive structure [33–35]. The above phenomenon improved the interphase bonding within the concrete and ultimately enhanced its flexibility.
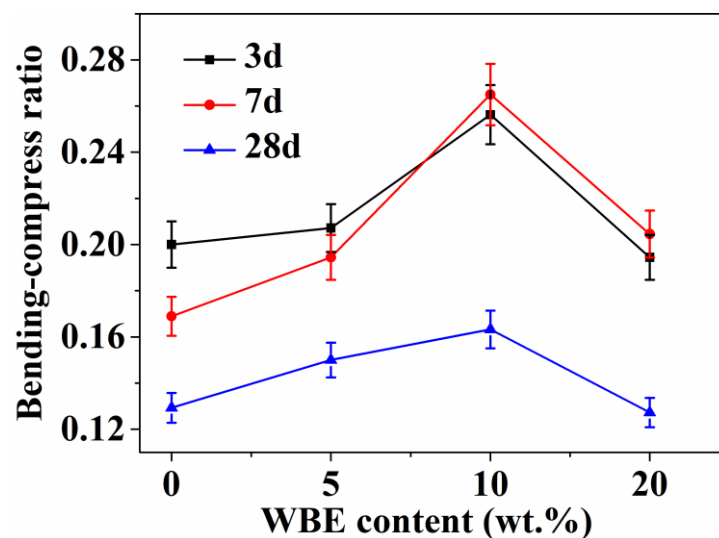

Figure 12. Effect of bending–compressive ratios of WBE-modified concrete with various curing times.

To further investigate the impact of WBE on the tensile strength and ultimate tensile strain of concrete, Figure 13 illustrates the 28-day tensile stress–strain curve of the modified concrete. The fracture behavior of all concrete specimens was single-joint cracking, with no notable occurrence of multi-joint cracking. Plain concrete (CF) demonstrated an average tensile strength and tensile strain of 3.58 MPa and 111.32 $\mu\varepsilon$, respectively. However, the

incorporation of WBE-modified concrete (W5CF, W10CF, and W20CF) resulted in improved tensile strength. Specifically, the average tensile strength of W5CF, W10CF, and W20CF increased to 4.22 MPa (an increase of approximately 17.8%), 4.76 MPa (an increase of approximately 32.9%), and 5.45 MPa (an increase of approximately 52.2%), respectively. Similarly, the stress–strain curves exhibited an increase in the ultimate tensile strain of W5CF, W10CF, and W20CF to 164.76 $\mu\varepsilon$ (an increase of approximately 48%), 340.67 $\mu\varepsilon$ (an increase of approximately 206%), and 412.83 $\mu\varepsilon$ (an increase of approximately 270%), respectively. The results from the flexural and tensile tests highlighted two critical observations: the water-based epoxy WBE remarkably enhanced the ductility of the concrete during the elastic phase, and a 10% WBE admixture was the turning point to improve the flexural and tensile strength of the concrete. Furthermore, the incorporation of fiber components had a strong impact on enhancing the ductility and tensile properties of the concrete, as demonstrated by the synergistic promotion of tensile strength and ultimate tensile strain. In the concrete system, WBE improved the bond strength between the cementitious materials and aggregates, enhancing the interface transition zone. It also reduced brittle cracking in the interface, ultimately improving the tensile strength of the concrete [36,37]. Moreover, under the protection of WBE, the fiber component was safeguarded against corrosion damage from the high-alkaline environment and the cutting damage of the crystal edges, resulting in a prominent bonding and wrapping force on the fiber surface [38,39]. The combined effects of the WBE and the fiber component mutually promoted each other, obtaining an advance in the tensile strength and ductility of the concrete.
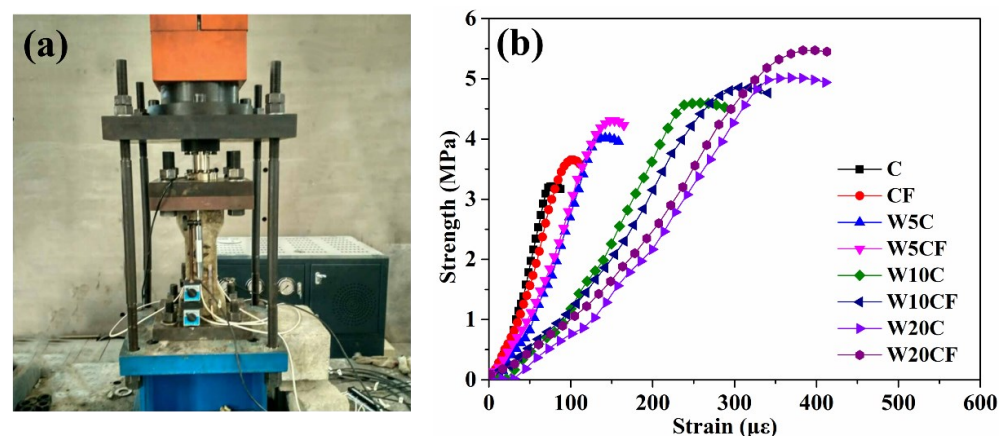

Figure 13. (**a**) Concrete axial tensile strength test, (**b**) 28-day tensile stress–strain curve of WBE-modified concrete.

Figure 14 presents the bond strength assessment of the WBE-modified concrete specimens after 28 days of curing. The bond strength was evaluated using positive tensile bond and split tensile bond measurements. The results demonstrated a positive association between the bond strength and the quantity of WBE. For instance, the positive tensile bond strength of the control concrete (CF) was 1.56 MPa, while that of the W5CF, W10CF, and W20CF specimens increased to 2.37 MPa (51.9% increase), 2.64 MPa (69.2% increase), and 2.84 MPa (82.1% increase), respectively. These findings implied that the utilization of WBE effectively enhanced the bonding strength between the old and new interfaces of the concrete.

3.3. Durability Testing of WBE-Modified Concrete

Upon microscopic analysis, it has been observed that the introduction of WBE into the cement paste led to an increase in the paste viscosity via the entrapment of gas during the mixing process, subsequently resulting in an augmentation of the matrix porosity. In contrast, when WBE was employed in forming the spatial network structure, it filled in the pores and impeded the movement of the liquid phase and ion transport. Therefore, the

diffusion coefficient of chloride ions was a crucial parameter to evaluate the longevity and safety of the concrete. The lower the diffusion coefficient of chloride ions, the greater the concrete's resilience to chloride ion corrosion, thus emphasizing the significance of these parameters in assessing the durability of concrete [40,41].
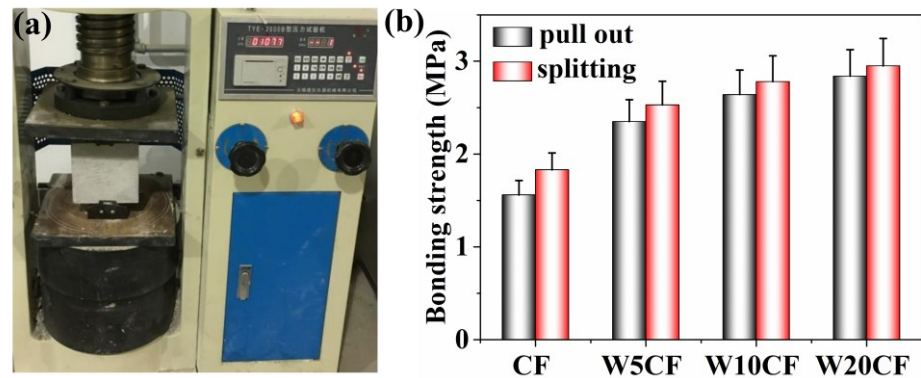

Figure 14. (**a**) The interface bond strength test loading equipment, (**b**) The interface bond strength of various WBE-modified concrete samples with curing age of 28 days.

Figure 15 illustrates the chloride diffusion coefficients of WBE-modified concrete at different curing times. The chloride diffusion coefficient reduced with an elongation in the curing time. Specifically, at 28 days, the chloride diffusion coefficients of C, W5C, W10C, and W20C were 8.4×10^{-12}, 5.0×10^{-12}, 2.2×10^{-12}, and 3.3×10^{-12} m^2/s, respectively, while the chloride diffusion coefficients of CF, W5CF, W10CF, and W20CF were 8.8×10^{-12}, 5.2×10^{-12}, 2.3×10^{-12}, and 3.5×10^{-12} m^2/s, respectively. This reduction in values can be attributed to the sufficient hydration reaction, diminishing the porosity and raising the density of the concrete, resulting in impeded diffusion for the chloride ions. Moreover, after the addition of the WBE admixture, the chloride diffusion coefficient of the concrete displayed a descending and subsequently an ascending trend. The minimum diffusion coefficient was observed in the concrete with a 10% (mass) admixture of WBE at 3, 7, and 28 days of curing. Owing to the improved microscopic morphology and density of the concrete resulting from the admixture of WBE, the diffusion rate of chloride ions was considerably reduced. As SEM images reveal in Figure 5, WBE remarkably improved the microscopic morphology of the concrete, which reduced the density of the pores in concrete, thereby decreasing the diffusion rate of chloride ions. Furthermore, the addition of WBE accelerated the hydration reaction, resulting in the production of a CH hydration product, which physically adsorbed the chloride ions, producing calcium hypochlorite and calcium chloride. The presence of these compounds lowered the proportion of free chloride ions and the electromigration in the concrete, thereby enhancing the corrosion resistance of the concrete to chloride ions [42,43].
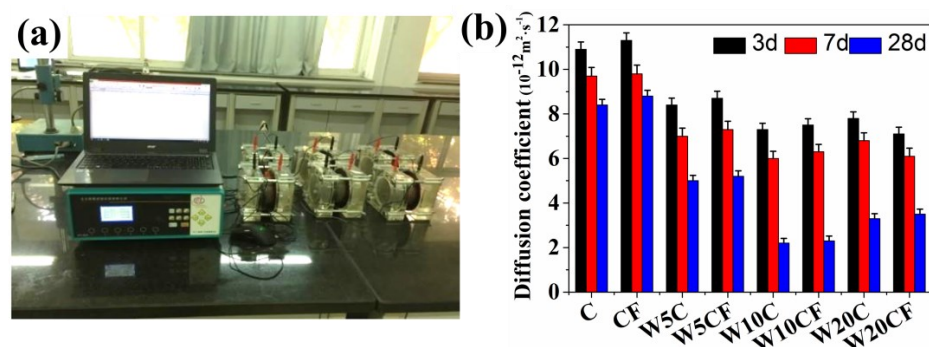

Figure 15. (**a**) Chloride ion flux test instrument, (**b**) chloride ion diffusion coefficient results of WBE-modified concrete of various curing ages.

Additionally, the epoxy resin filler possessed an abundance of hydroxyl- and oxygen-containing functional groups, which exhibited strong water absorption and enabled certain adsorption and the binding of chloride ions. This was beneficial to the adsorption of chloride ions, hindering their diffusion and generating a reduction in the chloride ion diffusion coefficient. However, when the WBE reached 20% (W20CF), the diffusion coefficient in the erosion solution tended to ascend due to the excessive addition of WBE, which brought forth a large amount of gas in fresh concrete, forming bubbles. After concrete hardening, these bubbles formed more pores that seriously weakened the continuity and impermeability of the cement paste, rendering it easier for erosion ions to penetrate the cement interior. The reaction between the erosion ions and cement hydration products caused swelling, along with the reduced alkalinity of the cement and the decomposition of hydration products such as C-S-H gels, ultimately causing a reduction in the concrete strength. Furthermore, comparing the chloride ion diffusion coefficients of the WBE-modified concretes before and after the addition of fiber, it was revealed that the fiber's effect on the permeability was more pronounced. The incorporation of fiber promoted the migration of chloride ions into the concrete matrix. Given that the carbon fiber primarily existed in bundles in the cement hardening slurry, an interfacial transition zone within the slurry produced a fast ion channel. Thus, the fiber component facilitated the migration capability of the chloride ions and reduced the permeability of the concrete. According to the concrete durability test and evaluation methods, the chloride ion permeability resistance level of ordinary concrete is RCM-I. However, when the WBE amount exceeded 10%, the chloride ion permeability level of the concrete could reach RCM-III to RCM-IV.

The assessment of concrete durability relied significantly on the frost resistance of the concrete. Quality loss tests of the WBE-modified concrete at varying freeze–thaw cycles are presented in Table 5 after varying numbers of freeze–thaw cycles (0–300). The results clarified that concrete quality progressively deteriorates with an increasing number of freeze–thaw cycles, primarily attributable to the water absorption reaching saturation and the freeze–thaw cycles causing damage within concrete. The freezing of internal water molecules generated stresses that resulted in the accumulation of cyclic damage inside the concrete, and the appearance of surface shedding. These phenomena obviously became more severe as the number of freeze–thaw cycles increased, coupled with a gradual increase in quality loss. When the number of freeze–thaw cycles reached 300, the mass loss rate of CF, W5CF, W10CF, and W20CF was 0.72%, 0.56%, 0.21%, and 0.37%, respectively. Notably, W10CF had the lowest mass loss of 0.21%, illustrating the highest frost resistance. The improved frost resistance can be attributed to the WBE's promoting effect on the hydration reaction, obtaining a more compact structure of hydration products with reduced pores and cracks, and better distribution uniformity [44,45]. The average mass loss of all the concrete specimens after 300 freeze–thaw cycles was less than 1%, which was remarkably less than 60% as stipulated in standard GB/T 50082-2009, suggesting the superior quality of the obtained concrete.

Table 5. Mass loss of WBE-modified concrete in freeze–thaw cycles.

Sample	Concrete Mass Loss					
	0	25	50	100	200	300
C	0	0.29	0.39	0.46	0.57	0.87
CF	0	0.28	0.33	0.39	0.49	0.72
W5C	0	0.23	0.29	0.37	0.47	0.66
W5CF	0	0.20	0.24	0.33	0.42	0.56
W10C	0	0.08	0.15	0.19	0.23	0.25
W10CF	0	0.06	0.12	0.18	0.20	0.21
W20C	0	0.16	0.24	0.28	0.33	0.39
W20CF	0	0.12	0.16	0.21	0.26	0.37

Figure 16 presents images of the WBE-modified concrete specimens after 25, 100, and 300 freeze–thaw cycles. The surface of the plain concrete (CF) exhibited spalling and blurring surface features after 25 cycles, and subsequent cycles led to the release of coarse aggregates and a substantial loss of surface cementite. After 300 cycles, coarse aggregates were exposed on the surface. In comparison, W5CF showed no significant freeze–thaw damage after the first 200 cycles, with no spalling marks on the surface. However, after 300 cycles, some cement stones at the edges of the air holes on the surface of the specimen were dislodged due to the crystallization expansion force inside the holes, while the rest of specimen remained unaffected. The specimen of W10CF displayed no noteworthy changes in its surface morphology after 300 cycles. These observations revealed that the application of WBE substantially enhanced the frost resistance of concrete.
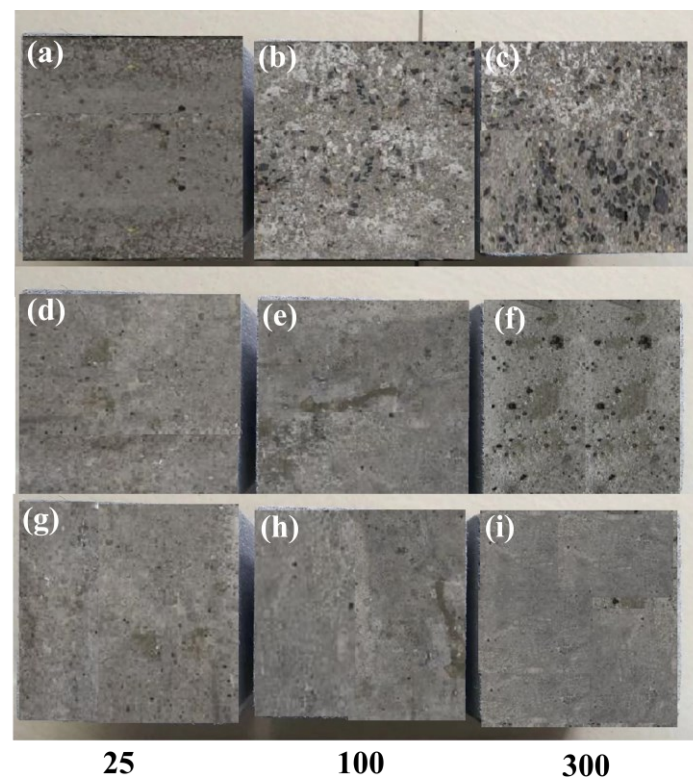

Figure 16. Photos of WBE-modified concrete specimen after 25, 100, 300 freeze–thaw cycles, (**a–c**) CF, (**d–f**) W5CF, (**g–i**) W10CF.

Figure 17 depicts the variation in the relative kinematic modulus of concrete modified with WBE under varying numbers of freeze–thaw cycles. The results displayed a continuous decrease in the relative dynamic elastic modulus with an increase in the freeze–thaw cycles. The fastest rate of decline was observed when without the WBE admixture. The relative dynamic elasticity modulus of CF, W5CF, W10CF and W20CF was 82.14%, 90.07%, 94.86%, and 92.04% after 300 freeze–thaw cycles, respectively, demonstrating the most significant loss of relative dynamic elastic modulus in the absence of WBE. Notably, W10CF exhibited the maximum relative dynamic elastic modulus of 94.86%, which was 7.51% higher than that of CF. The value increment could be attributed to two main factors. Firstly, WBE enhanced the microstructure of the concrete by reducing the number of cracks and gaps, thereby increasing its density. Secondly, the addition of WBE expedited the hydration reaction, leading to the formation of hydration products such as CH, which filled the capillary pores of the concrete, lowered the amount of free water, and consequently raised the dynamic modulus of elasticity [46].
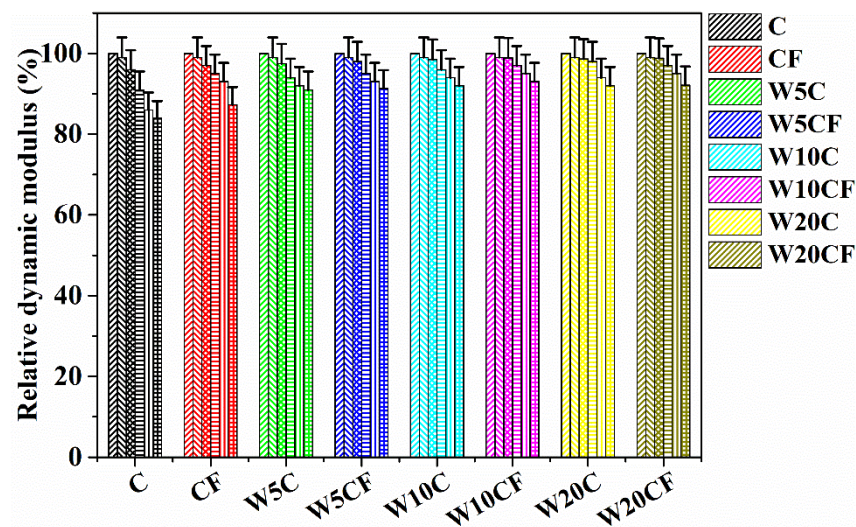
Figure 17. Relative dynamic elastic modulus of WBE-modified concrete after the freeze–thaw cycles, The number of cycles are 0, 25, 50, 100, 200, 300, respectively.

Figure 18 displays the drying shrinkage experiment conducted on the WBE-modified concrete. The results illustrated that the 28-day shrinkage value of the reference concrete ranged from 400–500 $\mu\varepsilon$, and the 1-year shrinkage value was about 530 $\mu\varepsilon$. In contrast, the 28-day shrinkage value of W10CF and W20CF was in the range of 200–300 $\mu\varepsilon$ and 100–200 $\mu\varepsilon$, and the 1-year shrinkage value was around 420 $\mu\varepsilon$ and 335 $\mu\varepsilon$, implying a reduction of 20.7% and 31.1%, respectively, in comparison to the control group. Overall, the utilization of WBE led to a decrease in the drying shrinkage of the concrete. The shrinkage reduction effect resulted from two aspects. Firstly, WBE conducted polymerization without by-products, which resulted in negligible volume shrinkage without water evaporation. In contrast, the hydration of cement was accompanied by both drying and chemical shrinkage. Therefore, a higher proportion of WBE in the mixture decreased the proportion of cement, ultimately resulting in less shrinkage. Secondly, as for ordinary concrete, the evaporation of water from the surface caused a decrease in the surface humidity while the internal humidity increased. Consequently, the dry shrinkage stress extended from the surface to the interior of the concrete, resulting in tensile stress on the surface and compressive stress in the interior. When the tensile stress surpassed the ultimate tensile strength, shrinkage cracks appeared. By adding WBE to the concrete mixture, the coated surface of the concrete delayed the evaporation of water and reduced the difference between the internal and external humidity levels, ultimately observing a reduction in the drying shrinkage [47].
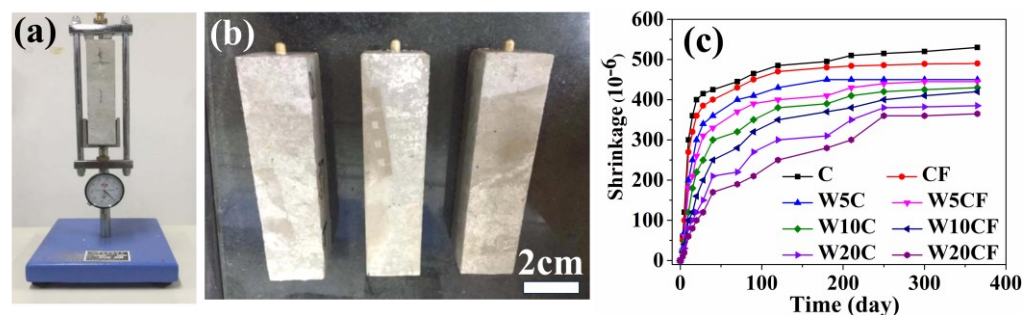

Figure 18. (**a**) Vertical dry shrinkage instrument, (**b**) samples, (**c**) the drying shrinkage of WBE-modified concrete of various curing ages.

From an economic point of view, as seen in Table 6, the polymer-modified cement concrete formulated using carbon nanofibers and epoxy resin is now compared to calculate the economic cost budgets of ordinary concrete and polymer-modified concrete based on

the current market prices of various materials. In this case, the dosage of epoxy resin and carbon nanofibers is 10% and 1%, respectively. It is found that the cost price of epoxy-modified cement concrete is 170 USD/m^3, which is nearly three times that of plain concrete. However, the mechanical properties of polymer-modified cement concrete, such as 28-day compressive strength, flexural strength, tensile strength and bond strength, were significantly improved compared with plain concrete. Meanwhile, the durability performance indexes such as chlorine penetration resistance, freeze–thaw cycle mass loss, relative dynamic modulus of elasticity, and drying shrinkage were remarkably enhanced compared with that of plain concrete. Therefore, fiber- and polymer-modified concrete extends the service life of concrete structures, thus saving manpower and materials, is cost-effective, and provides the advantage of long-lasting savings.

Table 6. Comparative analysis of costs and performance of plain concrete and polymer concrete.

Items	Plain Concrete	Polymer Concrete
Polymer dosing (%)	0	10
Carbon fiber dosing (%)	0	1
Cost (USD/m^3)	55	170
Compressive strength for 28 days (MPa)	58.2	55.4
Flexural strength for 28 days (MPa)	7.5	8.1
Tensile strength (MPa)	3.58	4.76
Bond strength (MPa)	1.56	2.64
Chloride permeation resistance grade	RCM-I	RCM-III
Mass loss of freeze–thaw cycles (%)	0.87	0.21
Relative dynamic elastic modulus (%)	82.14	93.86
Drying shrinkage after one year ($\mu\varepsilon$)	530	420

4. Conclusions

This research study examined the synergistic effects of carbon-nanofiber- and epoxy-resin-reinforced concrete. The mechanical and durability performance of the specimens in a cured state were researched at three different curing ages, i.e., 3, 7, and 28 days. The water-based epoxy WBE content was changed between three dosing levels of 5%, 10%, and 20%. The axial compressive behavior, axial stress strain response, flexural strength, and ductility behavior of the specimens were also assessed. The durability properties of the WBE-modified concrete were investigated via evaluation of its permeability, frost resistance, and volume stability. The mechanisms of WBE and carbon nanofiber synergy on the improvement of concrete performance were systematically studied. Based on the results, the following primary conclusions were drawn:

(1) The addition of epoxy resin WBE to cement raw materials resulted in an increasing consumption of C_3S and C_2S, accelerating the formation of CH and other hydration products, and enhancing the interconnectivity between the hydration products. Finally, a significant reduction in the number of pores and cracks was realized. The most compact concrete structure and minimal cracks were achieved with a WBE ratio of 10%.

(2) Concrete mixed with WBE exhibited a decreasing trend in compressive strength and elasticity modulus and a rising trend in Poisson's ratio at all curing ages. The fiber component revealed no remarkable effect on Poisson's ratio. An increase in the WBE content added showed a downward trend in the elasticity modulus for the WBE-modified concrete. As a critical factor, WBE enhanced the ductility of the concrete, while the fiber component exhibited a more obvious impact on the crack resistance and toughening with the cooperation of WBE.

(3) The flexural strength and flexural–compression ratio of the WBE-modified concrete showed an ascending and then descending trend with the addition of WBE. The maximum flexural strength of concrete was observed with 10% WBE content, attributable to the incorporation of aggregate and hydration products to form an elastic

organic–inorganic composite mesh structure in virtue of a WBE film. Beyond 10% WBE, the enhancement in the flexural capacity was reduced due to defects and the stress concentration point of WBE. The improved interphase forces within the concrete further strengthened the flexibility and crack resistance of the modified concrete.

(4)   The lowest value for the chloride ion diffusion coefficient of concrete was obtained with 2.2×10^{-12} m^2/s at 28 days curing time and with a 10% admixture of WBE. The concrete permeability was classified as RCM-III to RCM-IV.

(5)   Due to the improvement in the freeze–thaw cycle properties of WBE with carbon fiber incorporation, a lowest mass loss rate of 0.21% and a maximum value of relative dynamic elastic modulus of 94.86% under 300 freeze–thaw cycles were achieved for the W10CF sample. The "cracking effect" of the carbon fiber was more pronounced, whereas the "filling effect" of the WBE was more noticeable. WBE exhibited a favorable optimization effect on the pore structure of concrete, resulting in a reduced number of cracks and gaps, increased densities, and remarkable improvements in frost resistance.

(6)   The impermeability, frost resistance, and volume stability of the WBE-modified concrete composites were positively correlated with the WBE amount. Carbon fiber had a negative effect on the permeability of the concrete, but no notable influence on its frost resistance and volume stability.

(7)   Fiber- and resin-modified concrete has a wide range of applications in practical applications such as building structures, road engineering, bridge construction, etc., with the advantages of improved structural performance, enhanced durability, and reduced maintenance costs. Also, strict quality control and testing are required to ensure that the quality and performance of the modified concrete is in accordance with the requirements.

References

1.   Zheng, Y.X.; Zhang, Y.; Zhuo, J.B.; Zhang, Y.M.; Wan, C. A review of the mechanical properties and durability of basalt fiber-reinforced concrete. *Constr. Build. Mater.* **2022**, *359*, 129360. [CrossRef]
2.   Shao, R.Z.; Wu, C.Q.; Li, J. A comprehensive review on dry concrete: Application, raw material, preparation, mechanical, smart and durability performance. *J. Build. Eng.* **2022**, *55*, 104676. [CrossRef]
3.   Yi, J.; Wang, L.; Ma, L.J.; Zhang, Q.C.; Zhang, J.W.; Chi, J.S. Experimental study on basic mechanical properties of PVA fiber-reinforced coral cement-based composites. *Materials* **2023**, *16*, 2914. [CrossRef]
4.   Golewski, G.L. Concrete composites based on quaternary blended cements with a reduced width of initial microcracks. *Appl. Sci.* **2023**, *13*, 7338. [CrossRef]
5.   Zhang, T.H.; Mahdi, M.; Issa, M.; Xu, C.X.; Ozevin, D. Experimental study on monitoring damage progression of basalt-FRP reinforced concrete slabs using acoustic emission and machine learning. *Sensors* **2023**, *23*, 8356. [CrossRef] [PubMed]
6.   Hou, D.S.; Chen, D.D.; Wang, X.P.; Wu, D.; Ma, H.Y.; Hu, X.X.; Zhang, Y.; Wang, P.; Yu, R. RSM-based modelling and optimization of magnesium phosphate cement-based rapid-repair materials. *Constr. Build. Mater.* **2020**, *263*, 120190. [CrossRef]
7.   Li, J.S.; Zhang, W.B.; Cao, Y. Laboratory evaluation of magnesium phosphate cement paste and mortar for rapid repair of cement concrete pavement. *Constr. Build. Mater.* **2014**, *58*, 122–128. [CrossRef]
8.   Haruna, S.I.; Zhu, H.; Jiang, W.L.X.; Shao, J.W. Evaluation of impact resistance properties of polyurethane-based polymer concrete for the repair of runway subjected to repeated drop-weight impact test. *Constr. Build. Mater.* **2014**, *309*, 125152. [CrossRef]

9.   Jung, K.C.; Roh, I.T.; Chang, S.H. Evaluation of mechanical properties of polymer concretes for the rapid repair of runways. *Compos. B Eng.* **2014**, *58*, 352–360. [CrossRef]

10. Shi, C.; Zou, X.W.; Yang, L.; Wang, P.; Niu, M.D. Influence of humidity on the mechanical properties of polymer-modified cement-based repair materials. *Constr. Build. Mater.* **2020**, *261*, 119928. [CrossRef]

11. Liu, F.; Pan, B.F.; Zhou, C.J. Experimental study on a novel modified magnesium phosphate cement mortar used for rapid repair of portland cement concrete pavement in seasonally frozen areas. *J. Mater. Civ. Eng.* **2022**, *34*, 04021483. [CrossRef]

12. Aykac1, S.; Kalkan, I.; Aff, S.E.; Aykac, B.; Karahan, S.; Kaya, S. Strengthening and repair of reinforced concrete beams using external steel plates. *J. Struct. Eng.* **2013**, *139*, 929–939. [CrossRef]

13. Tayeh, B.A.; Bakar, B.H.A.; Johari, M.A.M. Characterization of the interfacial bond between old concrete substrate and ultrahigh performance fiber concrete repair composite. *Mater. Struct.* **2013**, *46*, 743–753. [CrossRef]

14. Wang, Y.M.; Wang, C.D.; Zhou, S.H.; Liu, K.W. Influence of cationic epoxy resin type on electrophoretic deposition effect on repair of rust-cracked reinforced concrete. *Constr. Build. Mater.* **2022**, *324*, 126714. [CrossRef]

15. Hang, Z.Y.; He, K.S.; Zhao, W.; Yu, Y. Fracture properties of a concrete-epoxy mortar interface with precoating treatment applied through image correlation technology. *Constr. Build. Mater.* **2023**, *370*, 130640. [CrossRef]

16. Hawary, M.E.; Khaiat, H.A.; Fereig, S. Performance of epoxy-repaired concrete in a marine environment. *Cem. Concr. Res.* **2000**, *30*, 259–266. [CrossRef]

17. Pang, B.; Jin, Z.Q.; Zhang, Y.S.; Xu, L.; Li, M.Y.; Wang, C.C.; Zhang, Y.; Yang, Y.; Zhao, P.; Bi, J.X.; et al. Ultraductile waterborne epoxy-concrete composite repair material: Epoxy-fiber synergistic effect on flexural and tensile performance. *Cem. Concr. Res.* **2022**, *129*, 104463. [CrossRef]

18. Wang, C.D.; Wang, Y.M.; Liu, K.W.; Zhou, S.H. Effect of colloid solution concentration of epoxy resin on properties of rust-cracked reinforced concrete repaired by electrophoretic deposition. *Constr. Build. Mater.* **2022**, *318*, 126184. [CrossRef]

19. Guo, S.Y.; Zhang, X.; Chen, J.Z.; Mou, B.; Shang, H.S.; Wang, P.; Zhang, L.H.; Ren, J. Mechanical and interface bonding properties of epoxy resin reinforced Portland cement repairing mortar. *Constr. Build. Mater.* **2020**, *264*, 120715. [CrossRef]

20. Luo, J.L.; Li, Q.Y.; Zhao, T.J.; Gao, S.; Sun, S.W. Bonding and toughness properties of PVA fibre reinforced aqueous epoxy resin cement repair mortar. *Constr. Build. Mater.* **2013**, *49*, 766–771. [CrossRef]

21. Uzbas, B.; Aydin, A.C. Microstructural analysis of silica fume concrete with scanning electron microscopy and X-Ray diffraction. *Eng. Technol. Appl. Sci.* **2020**, *10*, 5845–5850. [CrossRef]

22. Li, Y.; Guo, Y.C.; Lyu, Z.H.; Wei, X. Investigation of the effect of waterborne epoxy resins on the hydration kinetics and performance of cement blends. *Constr. Build. Mater.* **2021**, *301*, 124045. [CrossRef]

23. Dai, Y.Q.; Yang, R.J.; Xu, C.J.; Mansour, A.A.; Lan, Y.; Peng, Y.; Li, L.; Zeng, Q.; Li, K.F. In-situ µ-XCT characterization of cement-waterborne epoxy resin coalescence. *Constr. Build. Mater.* **2023**, *377*, 131161. [CrossRef]

24. Liu, W.T.; Sun, Y.D.; Meng, X.X.; Qin, Y.Y. Experimental analysis of Nano-SiO$_2$ modified waterborne epoxy resin on the properties and microstructure of cement-based grouting materials. *Energy* **2023**, *268*, 126669. [CrossRef]

25. Byron, D.; Heitman, A.P.; Neves, J.; Souza, P.P.D.; Patricio, P.S.D.O. Evaluation of properties of polymer concrete based on epoxy resin and functionalized carbon nanotubes. *Constr. Build. Mater.* **2021**, *309*, 125155. [CrossRef]

26. Lin, C.H.; Yu, J. Research on improving polymer pervious concrete mechanical strength by adding EVA to UP resin binder material. *Constr. Build. Mater.* **2022**, *359*, 129416. [CrossRef]

27. Akın, M.H.; Polat, R. The effect of vehicle waste tires on the mechanical, hardness and stress-strain properties of polyester-based polymer concretes. *Constr. Build. Mater.* **2022**, *325*, 126741. [CrossRef]

28. Joseph, L.; Chakravarthi, E.K.; Jayanarayanan, K.; Mini, K.M. Nano filler incorporated epoxy based natural hybrid fiber confinement of concrete systems: Effect of fiber layers and nano filler addition. *Structures* **2023**, *51*, 320–331. [CrossRef]

29. Ulu, A.; Tutar, A.I.; Kurklu, A.; Cakir, F. Effect of excessive fiber reinforcement on mechanical properties of chopped glass fiber reinforced polymer concretes. *Constr. Build. Mater.* **2022**, *359*, 129486. [CrossRef]

30. Carrillo, J.; Ramirez, J.; Marriaga, J.L. Modulus of elasticity and Poisson's ratio of fiber-reinforced concrete in Colombia from ultrasonic pulse velocities. *J. Build. Eng.* **2019**, *23*, 18–26. [CrossRef]

31. Li, K.; Wei, Y.X.; Li, Y.P.; Li, Z.Q.; Zhu, J.T. Flexural behavior of reinforced concrete beams strengthened with high-strength stainless steel wire rope meshes reinforced ECC. *Constr. Build. Mater.* **2023**, *362*, 129627. [CrossRef]

32. Saeed, Y.M.; Aules, W.A.; Rad, F.N.; Raad, A.M. Tensile behavior of FRP anchors made from CFRP ropes epoxy-bonded to uncracked concrete for flexural strengthening of RC columns. *Case Stud. Constr. Mater.* **2020**, *13*, e00435. [CrossRef]

33. Gujar, P.; Hirshikesh, H.; Annabattula, R.K.; Ghosh, P. Structural to interfacial fracture transition in epoxy coated hydrating cement. *Constr. Build. Mater.* **2021**, *310*, 125128. [CrossRef]

34. Li, P.F.; Jiang, Z.S.; An, X.H.; Maekawa, K.; Du, S.L. Time-dependent retardation effect of epoxy latexes on cement hydration: Experiments and multi-component hydration model. *Constr. Build. Mater.* **2022**, *320*, 126282. [CrossRef]

35. Bahraq, A.A.; Obot, I.B.; Osta, M.A.A.; Amoudi, O.S.B.A.; Maslehuddin, M. Molecular-level investigation on the effect of surface moisture on the bonding behavior of cement-epoxy interface. *J. Build. Eng.* **2022**, *61*, 105299. [CrossRef]

36. Zhao, Q.; Zhang, D.X.; Zhao, X.L.; Sharma, S. Modelling damage evolution of carbon fiber-reinforced epoxy polymer composites in seawater sea sand concrete environment. *Compos. Sci. Technol.* **2021**, *215*, 108961. [CrossRef]

37. Hussain, Q.; Ruangrassamee, A.; Tangtermsirikul, S.; Joyklad, P. Behavior of concrete confined with epoxy bonded fiber ropes under axial load. *Constr. Build. Mater.* **2020**, *263*, 120093. [CrossRef]

38. Li, J.l.; Xie, J.H.; Liu, F.; Lu, Z.Y. A critical review and assessment for FRP-concrete bond systems with epoxy resin exposed to chloride environments. *Compos. Struct.* **2019**, *229*, 111372. [CrossRef]

39. Xue, Y.C.; Qian, Z.D. Development and performance evaluation of epoxy asphalt concrete modified with mineral fiber. *Constr. Build. Mater.* **2016**, *102*, 378–383. [CrossRef]

40. Spainhour, L.K.; Wootton, I.A. Corrosion process and abatement in reinforced concrete wrapped by fiber reinforced polymer. *Cem. Concr. Res.* **2008**, *30*, 535–543. [CrossRef]

41. Wang, D.H.; Gong, Q.N.; Yuan, Q.; Luo, S.R. Review of the properties of fiber-reinforced polymer-reinforced seawater-sea sand concrete. *J. Mater. Civ. Eng.* **2021**, *33*, 04021285. [CrossRef]

42. Zheng, W.; Chen, W.G.; Feng, T.; Li, W.Q.; Liu, X.T.; Dong, L.L.; Fu, Y.Q. Enhancing chloride ion penetration resistance into concrete by using graphene oxide reinforced waterborne epoxy coating. *Prog. Org. Coat.* **2020**, *138*, 105389. [CrossRef]

43. Zuo, J.D.; Li, H.B.; Dong, B.Q.; Luo, C.Y.; Chen, D.Z. Mechanical properties and resistance to chloride ion permeability of epoxy emulsion cement mortar reinforced by glass flake. *Constr. Build. Mater.* **2017**, *155*, 137–144. [CrossRef]

44. Yin, S.P.; Jing, L.; Yin, M.T.; Wang, B. Mechanical properties of textile reinforced concrete under chloride wet-dry and freeze-thaw cycle environments. *Cem. Concr. Res.* **2019**, *96*, 118–127. [CrossRef]

45. Mahmoud, F.A.; Mechling, J.M.; Shaban, M. Bond strength of different strengthening systems-Concrete elements under freeze-thaw cycles and salt water immersion exposure. *Constr. Build. Mater.* **2014**, *70*, 399–409. [CrossRef]

46. Ying, G.G.; Song, C.; Ren, J.; Guo, S.Y.; Nie, R.; Zhang, L.H. Mechanical and durability-related performance of graphene/epoxy resin and epoxy resin enhanced OPC mortar. *Constr. Build. Mater.* **2021**, *282*, 122644. [CrossRef]

47. Wang, Y.; Zhang, S.H.; Li, G.X.; Shi, X.M. Effects of alkali-treated recycled carbon fiber on the strength and free drying shrinkage of cementitious mortar. *J. Clean. Prod.* **2019**, *228*, 1187–1195. [CrossRef]